

## Supplemental Figure Titles and Legends

### Figure S1. Strategy and confirmation of CD163 knockout in MA-104 cells, related to Figure 2.

**(A)** Genomic organization of the first four exons of the *CD163* gene. The sequence in exon 3 that was targeted by the guide RNA is shown in red, with the protospacer adjacent motif (PAM) sequence in blue. **(B)** Western blotting of CD163 receptor expression in wild-type and single-cell knockout clones generated by the limiting dilution method. **(C)** CRISPR/Cas9 base editing was confirmed by Sanger sequencing of multiple cloned polymerase chain reaction (PCR) amplicons from wild-type and clone F11  $\Delta$ CD163 cell lines.

### Figure S2. Restoration of CD163 expression in CD163<sup>null</sup> Vero cells is sufficient for restoring infectious SHFV particle production, related to Figure 2.

**(A)** The *CD163* gene from Vero and MA-104 cells was cloned into retroviral expression vectors. Vero cells were transduced with CD163-encoding gammaretrovirus derived from Vero or MA-104 cells, or empty vector, and stable cell lines were generated following antibiotic selection. Stable cell lines were exposed to SHFV (multiplicity of infection [MOI] = 3) and cell supernatant was harvested 24 h post-exposure. Viral titers were assessed by plaque assay, and the data show the mean  $\pm$  standard error of the mean (SEM; one-way analysis of variance [ANOVA] with Dunnett's post-test \*\*\*\* $P < 0.0001$ ) from three independent experiments, with one replicate per experiment. Dotted lines represent the limit of detection for the assay. Lysates from cells were probed for expression of CD163 by western blotting. Actin beta served as a protein loading control. **(B)** Bright-field images of cells in panel A taken 24 h post-exposure to virus. SHFV, simian hemorrhagic fever virus.

### Figure S3. Transfection of wild-type rSHFV or cDNA launch plasmid encoding rSHFV-eGFP bypasses the requirement for CD163, related to Figure 3.

A newly developed flow cytometric assay based on fluorescence *in situ* hybridization ("FISH-Flow") was used to enumerate the percentage of cells containing intracellular SHFV genomic RNA. **(A)**

SHFV exposure of  $\Delta$ CD163 cells did not yield progeny SHFV (Figure 2B), but cells transfected with rSHFV-eGFP-encoding plasmid resulted in sustained virus RNA within cells. Cells were either mock-transfected (top) or transfected with rSHFV-eGFP-encoding plasmid (control, middle;  $\Delta$ CD163, bottom) and analyzed at 24, 48, and 72 h post-transfection. All flow cytometric events were gated on FSC x SSC properties, followed by singlet discrimination. FISH-Flow analysis quantified probe fluorescence for ATTO-633-conjugated SHFV ORF1a (viral RNA), relative to side scatter area (SSC-A). Data are representative of two independent experiments. **(B)** Percentage of viral RNA-positive cells in the dim (top left), bright (top right), and both dim and bright gates (bottom) for control (black circles) and  $\Delta$ CD163 (red circles)-transfected cells. **(C)** Viral titers from cell supernatants transfected with rSHFV were assessed by plaque assay; the data show the mean  $\pm$  standard error of the mean (SEM) from two independent transfection experiments. **(D)** Confirmation of the importance of CD163 during virion entry using rSHFV-eGFP. Flow cytometric analysis of eGFP-fluorescence in rSHFV-eGFP-encoding plasmid-transfected cells analyzed 72 h post-transfection. Cells were gated as described in panel A, and mock-transfected cells were used to denote the GFP+ gate. Data are representative of three independent experiments. **(E)** Percentage of eGFP-positive cells enumerated from panel D. **(F)** Viral titers were assessed by plaque assay from supernatants of cells transfected with rSHFV-eGFP; the data show the mean  $\pm$  SEM from three independent transfection experiments. **(B, C, F)** Two-way analysis of variance (ANOVA) with Sidak's post-test of control compared to  $\Delta$ CD163 cells ( $*P < 0.05$ ,  $**P < 0.01$ ,  $****P < 0.0001$ ). **(E)** Unpaired two-tailed t-test ( $****P < 0.0001$ ). In contrast to control cells, rSHFV was unable to seed a spreading infection in cells lacking CD163. Similar findings were demonstrated for rSHFV-eGFP, as examined by eGFP flow cytometry and plaque assays. SHFV, simian hemorrhagic fever virus; rSHFV, recombinant SHFV; cDNA, complementary DNA; rSHFV-eGFP, rSHFV expressing enhanced green fluorescent protein.

**Figure S4. SHFV infects MA-104 cells lacking CD163 but cannot spread to new cells, related to Figure 3.**

**(A)** CD163 expression in the indicated cell lines following cell surface staining (red) and intracellular staining (blue) was measured by flow cytometry. Shaded histograms are from unstained cells and denote the CD163-negative population. The CD163-positive region is indicated by a black line from the  $10^3$  to the  $10^4$  decade, and the percentage of cells within this decade was enumerated for all cell lines. Shown are representative histograms. Values indicate the mean percentage of CD163-expressing cells  $\pm$  standard error of the mean (SEM) from two independent experiments. APC, Allophycocyanin. Both wild-type and matched  $\Delta$ CD163 cells were exposed to SFHV and analyzed by a flow cytometric assay based on fluorescence *in situ* hybridization (FISH-Flow) **(B)** 1 h or **(C)** 6 h later. Samples were either mock-exposed or SHFV-exposed at increasing multiplicities of infection (MOIs; 1, 10, or 100 PFU per cell). All flow-cytometric events were gated on FSC x SSC properties, followed by singlet discrimination. A total of at least 50,000 events was collected within the singlet gate. FISH-Flow analysis quantified probe fluorescence for ATTO-633-conjugated SHFV ORF1a (viral RNA), relative to side scatter area (SSC-A). The percentage of RNA-positive cells falling into the dim or bright gates is denoted above the graphs. **(B)** At 1 h, an MOI-dependent shift of both wild-type and  $\Delta$ CD163 cells was observed into a dim RNA-positive gate, suggesting that SHFV indeed has mechanisms to enter cells in the absence of CD163. In a parallel experiment, the cells were harvested 6 h post-virus-exposure (when first evidence of cytopathic effects were noted). **(C)** In wild-type cells, an MOI-dependent shift in viral RNA-positive cells from the dim to bright gates was observed, likely indicating robust viral RNA amplification. However, viral RNA-positive  $\Delta$ CD163 cells were no longer detected, indicating viral RNA clearance. SHFV, simian hemorrhagic fever virus.

**Figure S5. CD163 bears signatures of positive natural selection, related to Figure 4.**

To detect evidence of positive (diversifying) selection in primate *CD163*. Testing for site-specific selective pressures was performed using the phylogenetic analysis using maximum-likelihood (PAML) program (Yang, 2007). **(A)** Cladogram of primates used in this analysis with corresponding National Center for Biotechnology Information (NCBI) sequence identifiers. **(B)** Positive selection among

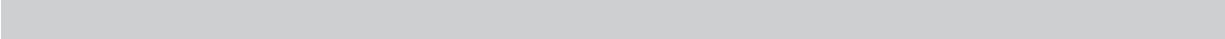
amino-acid sites was tested by two model comparisons, M7 vs. M8 and M8a vs. M8. In each of these comparisons, the null models (M7 and M8a, respectively) do not allow for sites under positive selection, whereas the alternative model (M8) does. Twice the difference in the natural logs of the likelihoods ( $2 \Delta \ln L$ ) is shown for each model comparison. A statistical comparison of the log-likelihood ratios from these models was highly significant ( $P < 0.01$ ), rejecting the null models in favor of the positive selection model. Residues shown correspond to codons assigned to the class with a dN/dS ratio of  $>1$  in M8 ( $P > 0.90$ ) by Bayes empirical Bayes (BEB) analysis. **(C)** Illustration of the CD163 receptor, showing the extracellular scavenger receptor cysteine-rich (SRCR domains 1–9), domains rich with proline serine threonine (PST) I and II, and the short cytoplasmic tail. The N-terminus (amine terminus;  $\text{NH}_2$ ) and C-terminus (carboxyl terminus;  $\text{COOH}$ ) denote the beginning and end of the protein polypeptide chain, respectively. **(D)** Linear domain diagram of the CD163 receptor with red tick marks denoting the location of codons under positive selection. Seven of the nine selected residues map to SRCR domains 6–9, an area that contains regions important to arterivirus infection (Gorp et al., 2010).

**Figure S6. Human macrophages are microscopically healthy following SHFV, but not Ebola virus, exposure, related to Figure 5.**

Monocytes were isolated from human peripheral blood mononuclear cells (PBMCs;  $n = 3$  donors) and differentiated into M0 macrophages. M0 macrophages were further polarized into M1 or M2 subsets using  $\text{IFN-}\gamma$  or IL-4, respectively. Monocyte-derived macrophages were exposed to SHFV (MOI = 3) or Ebola virus (MOI = 3). Exposures of MA-104 and Vero E6 cells served as cell line controls for SHFV and Ebola virus, respectively. Representative bright field images of cells were taken at 72 h post-exposure at 20X magnification. SHFV, simian hemorrhagic fever virus; EBOV, Ebola virus.

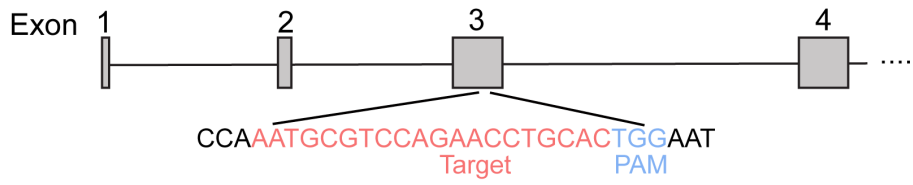
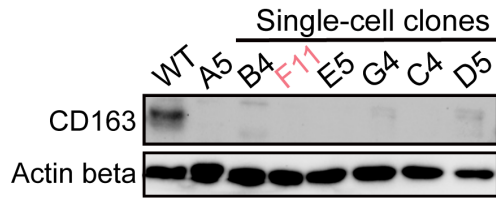
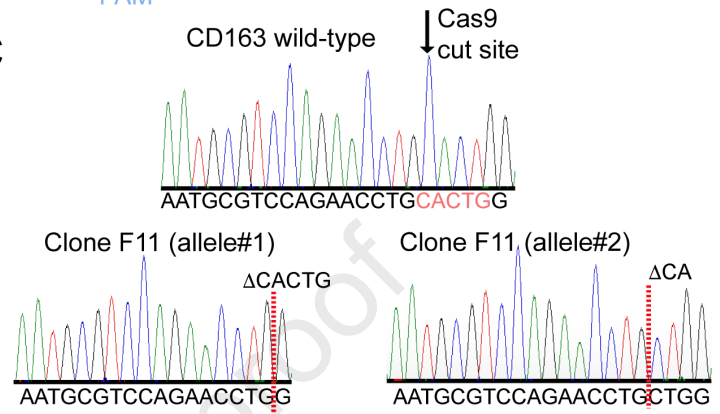
**Figure S7. CD163 protein expression is undetectable in all cell lines of the human NCI-60 cancer panel, related to Figure 6.**



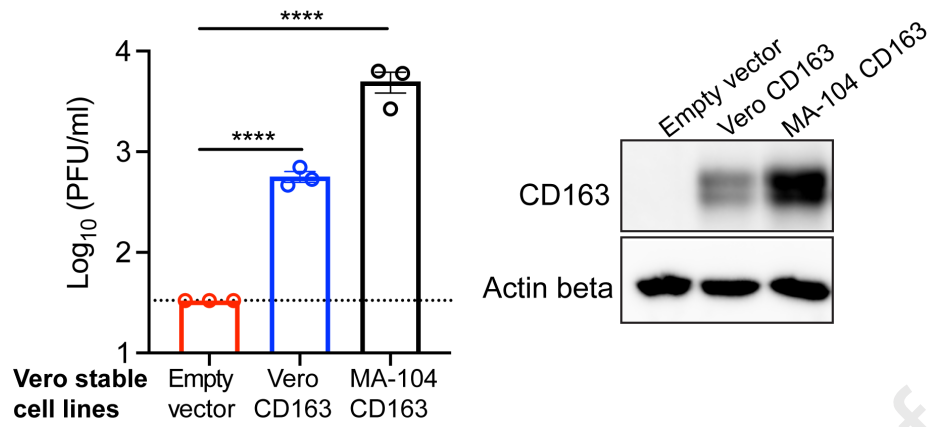
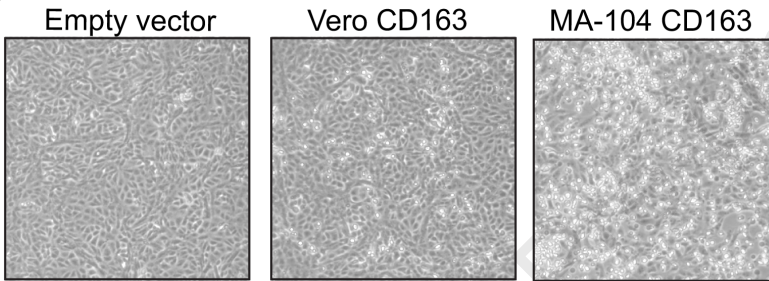


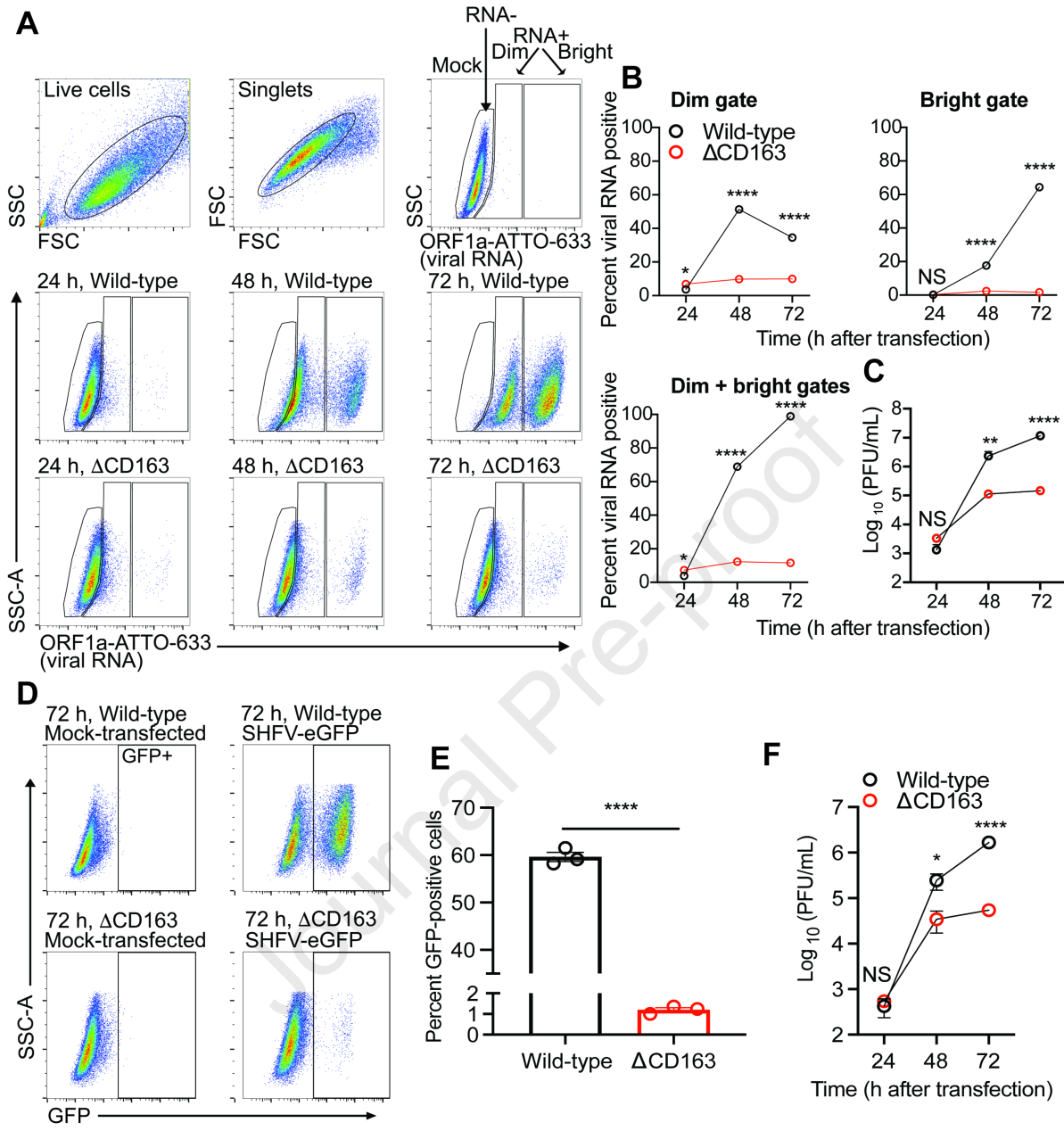
Expression of CD163 in grivet MA-104 cells permissive to simian hemorrhagic fever virus (SHFV) compared to cells of the human NCI-60 cancer panel by western blotting. A single 150-kDa band at the expected molecular weight (boxed insert in “CD163 blot”) for CD163 is denoted. Equivalent protein loading was ensured by total protein stain following transfer to a PVDF membrane (“stain-free blot”). All blots shown were photographed for a maximum of 5 min. CNS, central nervous system.

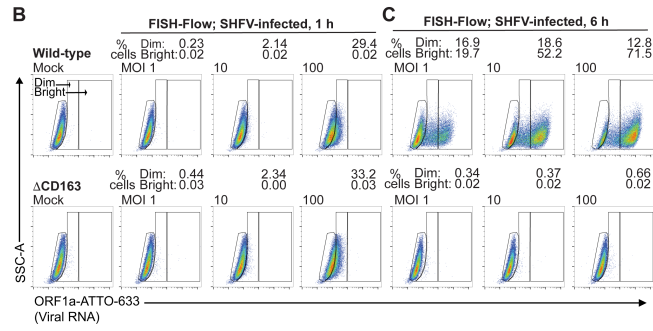
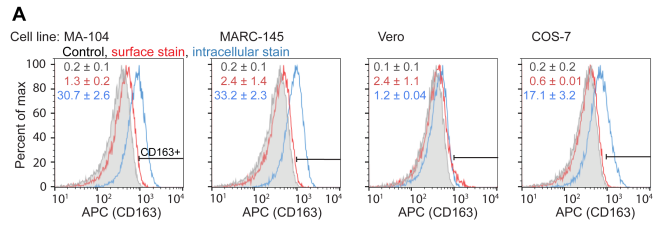
Journal Pre-proof

**A****B****C**

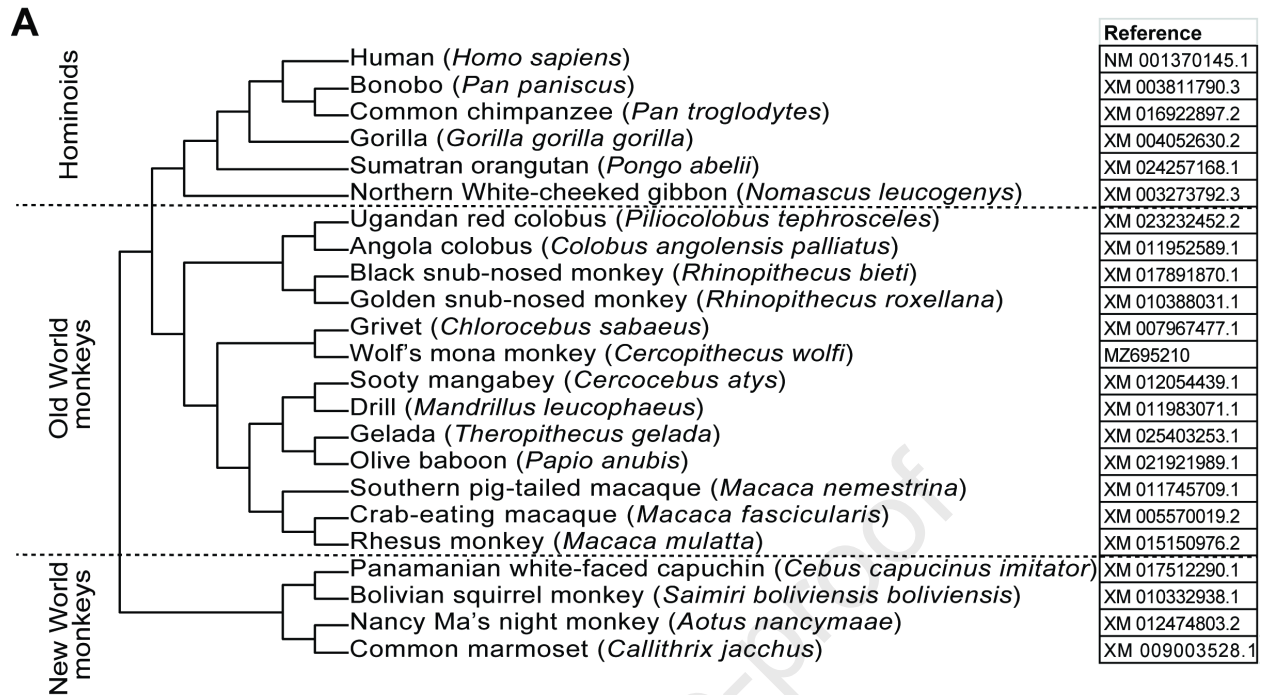
Journal Pre-proof

**A****B**



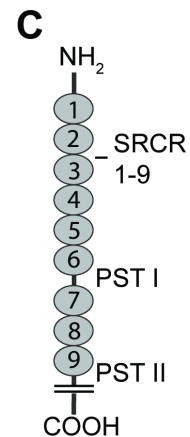
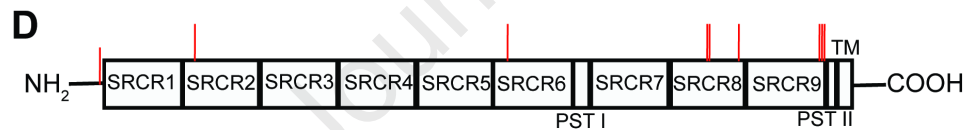


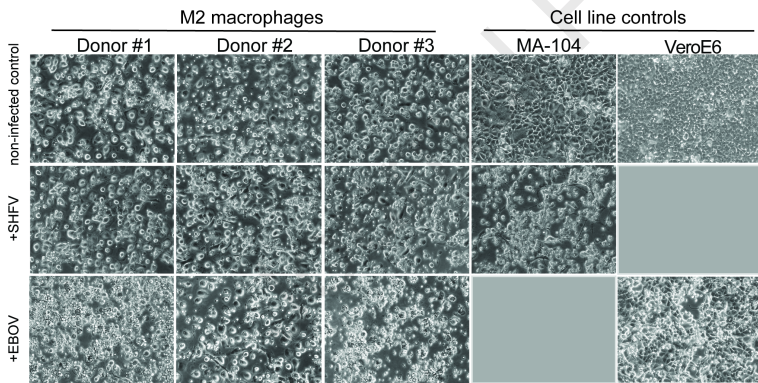
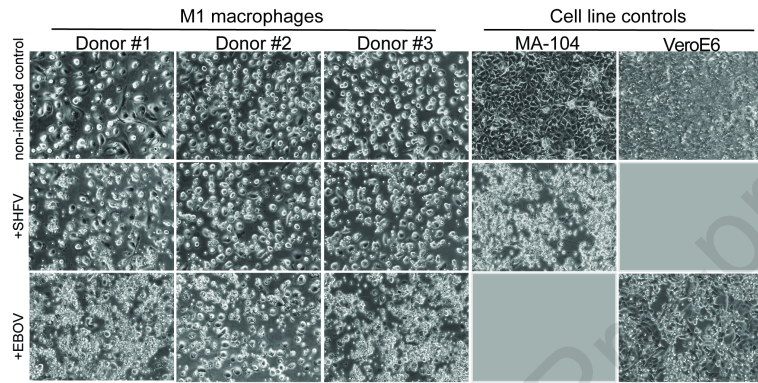
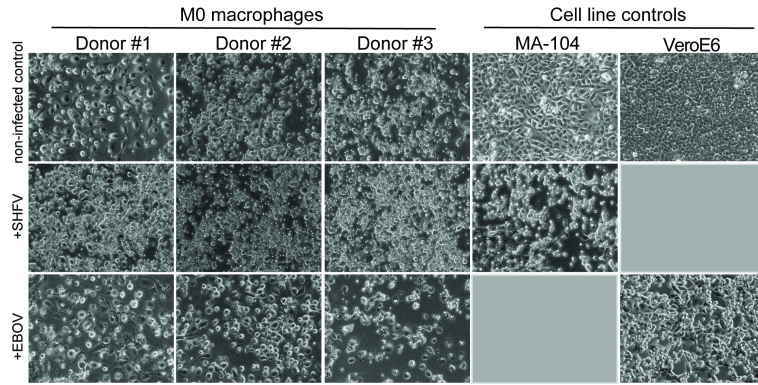
Journal Pre-proof



**B**

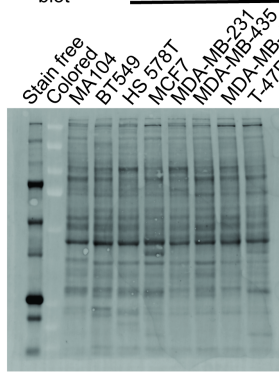
Gene	M7 vs M8		M8a vs M8		dN/dS value (% codons)	Residues under positive selection <i>P</i> > 0.9, * <i>P</i> > 0.95
	2ΔInL	<i>P</i> value	2ΔInL	<i>P</i> value		
<i>CD163</i>	11.61	<i>P</i> < 0.01	11.45	<i>P</i> < 0.001	2.8 (4.8%)	L44, R179, G602, P877, A878*, S918, D1030*, V1033, P1037



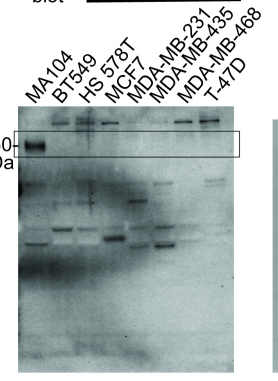




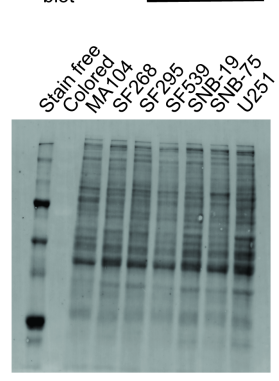
Stain-free blot Breast cancer



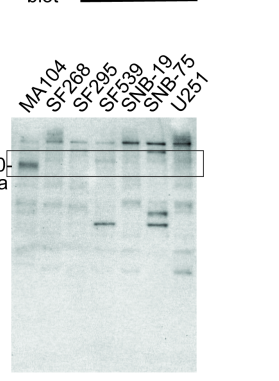
CD163 blot Breast cancer



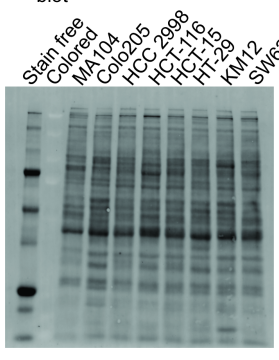
Stain-free blot CNS cancer



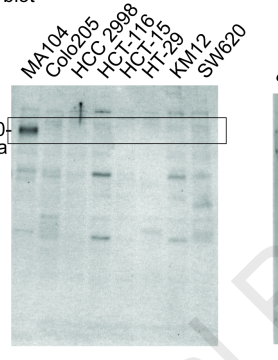
CD163 blot CNS cancer



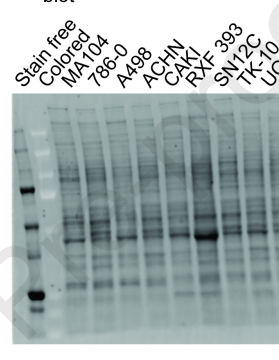
Stain-free blot Colon cancer



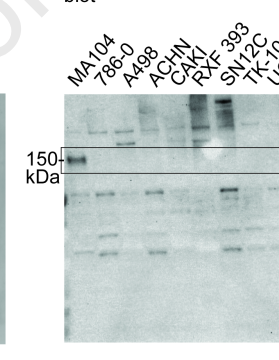
CD163 blot Colon cancer



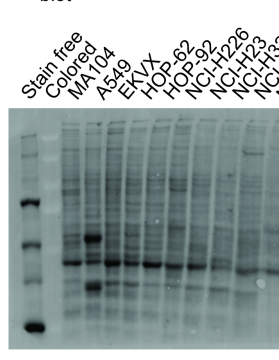
Stain-free blot Renal cancer



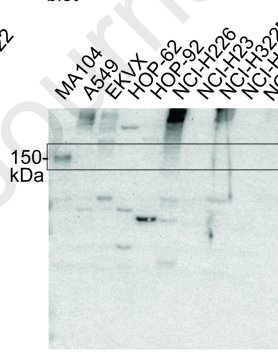
CD163 blot Renal cancer



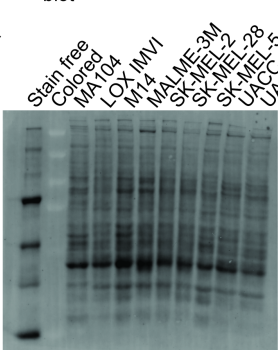
Stain-free blot Lung cancer



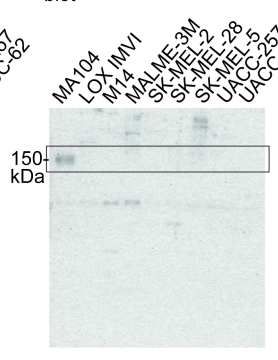
CD163 blot Lung cancer



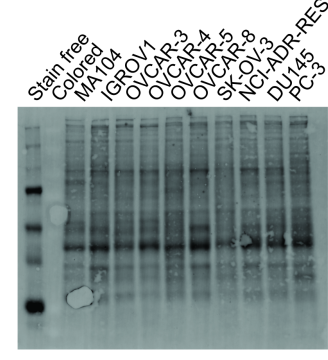
Stain-free blot Melanoma



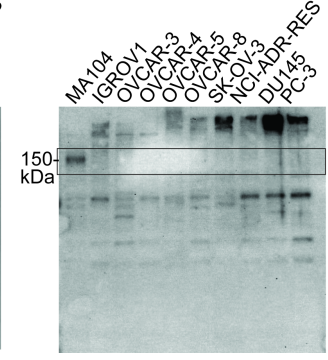
CD163 blot Melanoma



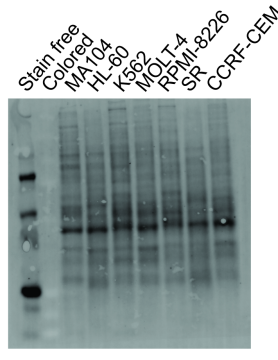
Stain-free blot Ovary Prostate



CD163 blot Ovary Prostate



Stain-free blot Leukemia



CD163 blot Leukemia

